Available online at www.sciencedirect.com
SCIENCE DIRECT®
Sensors and Actuators A 113 (2004) 1–11
SENSORS AND ACTUATORS A PHYSICAL
www.elsevier.com/locate/sna

Analysis of thin film piezoelectric microaccelerometer using analytical and finite element modeling

Qing-Ming Wang*, Zhaochun Yang, Fang Li, Patrick Smolinski

Department of Mechanical Engineering, University of Pittsburgh, 639 Benedum Hall, Pittsburgh, PA 15261, USA

Received 5 November 2003; received in revised form 11 February 2004; accepted 28 February 2004

Available online 24 May 2004

Abstract

Microaccelerometers using piezoelectric lead zirconate titanate (PZT) thin films have attracted much interest due to their simple structure and potentially high sensitivity. In this paper, we present a theoretical model for a microaccelerometer with four suspended flexural PZT-on-silicon beams and a central proof mass configuration. The model takes into account the effect of device geometry and elastic properties of the piezoelectric film, and agrees well with the results obtained by the finite element analysis. This study shows that the accelerometer sensitivity decreases with increases in the beam width, in the thickness of the bilayer beams, and in the elastic modulus of the mechanical microstructure. Increases in the beam length increase sensitivity. For a fixed beam thickness, a maximum sensitivity exists for appropriate PZT/Si thickness ratio. In addition, it is found that with appropriate geometrical dimensions, both high sensitivity and broad frequency bandwidth can be achieved. The calculation of the stress distribution in the suspended PZT/Si beam structure when the device is subjected to large vibrational acceleration indicates that the thin film microaccelerometer can stand extremely large *g* conditions with very good mechanical reliability. In the dynamic analysis, it is found that both analytical model and finite element modeling give very close results of the resonance frequency of the device. The results of this study can be readily applied to on-chip piezoelectric microaccelerometer design and its structural optimization.

Keywords: Piezoelectric accelerometer; MEMS; Sensitivity; Lead zirconate titanate (PZT) thin film

1. Introduction

Piezoelectric accelerometers use the direct piezoelectric effect of a piezoelectric ceramic, crystal or thin film to generate an electrical charge output that is proportional to applied acceleration [1–3]. In an accelerometer, the stress in the device occurs as a result of the seismic mass vibration imposing a force on the piezoelectric materials. The total amount of accumulated charge is proportional to the applied force and the applied force is proportional to acceleration. The electrodes on the piezoelectric device collect the charge that can be transmitted to a signal conditioner that is remote or built into the accelerometer. Once the charge is conditioned, the signal is available for display, recording, analysis or control as a varying voltage [2].

Piezoelectric accelerometers have the advantages of low cost, simple structure, easy integration with electronic circuitry, wide frequency response and high sensitivity. Thus, piezoelectric accelerometers have been widely used in condition monitoring systems to measure machinery vibration. Recently, microaccelerometers using piezoelectric thin film have drawn much research interest due to the miniaturization trend of electronic devices, their low cost and their suitability for batch manufacturing [4–7]. Research has focused on the thin film accelerometer design [8], fabrication [9], device's measurement capabilities [10] and structural analysis and modeling to increase the sensitivity of the devices. For example, Eichner et al. [11] have measured the mechanical vibration and electromechanical sensitivity of micromachined accelerometer devices with four piezoelectric read-out capacitors; Ries and Smith [12] have used the finite element method to analyze a deformable array transducer; and Yu and Lan [13] presented system modeling for the design of a microaccelerometer. However, it should be pointed out that all of these studies simply assume that the piezoelectric PZT thin films are very thin and can be neglected in the mechanical analysis. Considering that the thickness of PZT films deposited on-chip by sol–gel spin-on deposition, or screen printing are typically from 0.5 to 5 μm, even up to

* Corresponding author. Tel.: +1-412-6244885; fax: +1-412-6244846.
E-mail address: qmwang@engr.pitt.edu (Q.-M. Wang).

0924-4247/$ – see front matter © 2004 Elsevier B.V. All rights reserved.
doi:10.1016/j.sna.2004.02.041

20 μm [14,15], the effect of thickness and the elastic properties of piezoelectric films should be taken into consideration in structural analysis and device performance modeling. Inclusion of the effects of film thickness in analysis would provide a more accurate estimation of device performance and, therefore, would aid in device design.

The aim of this paper is to study both the static and dynamic behavior of the microaccelerometer accounting for the effect of PZT film thickness. Both an analytical and a computational model are developed and the results are compared. Using the analytical model, the effects of device geometry and the elastic properties of PZT thin film on the sensitivity of the accelerometer are evaluated. The results of this analysis can be used as a base for thin film piezoelectric microaccelerometer design and performance optimization.

2. Analytical models of thin film piezoelectric accelerometer

2.1. Static analysis

Generally, the two important parameters in evaluating accelerometer sensors are sensitivity and operating frequency range. Sensitivity can be defined as the generative charge per applied acceleration. Operating frequency range is the flat frequency response region below the fundamental resonance frequency of the sensor. We consider a microaccelerometer configuration with four suspended symmetric beams and a central proof mass. The PZT thin film on each flexural beam is patterned into two transducer elements, thus eight piezoelectric transducers are arranged on four beams symmetrically to form the sensing devices in the structures, as shown in Fig. 1. Yu and Lan [13] have adopted a similar configuration in their device analysis. When the central mass is subjected to vertical vibration (acceleration), the suspending flexural beam structure can effectively convert and amplify the vertical force (or vibration) of the central mass into the planar stress in the transverse direction of the piezoelectric PZT thin film elements, thus, greatly enhance the sensitivity of the device. Each piezoelectric transducer is composed of an upper electrode, a piezoelectric thin film and a lower electrode. The two PZT elements on each beam are poled in opposite directions along the thickness. To collect the generative electric charge from the thin film piezoelectric elements when the accelerometer is subjected to an applied acceleration, the two PZT thin film transducer elements on each beam can be connected electrically either in parallel or in series. In the case of series connection, the two PZT thin film elements are connected through the lower electrodes, while output electrical terminals (connections) are made through the two top electrodes, as shown in Fig. 2(a). Since, the stresses of the two PZT elements are in the opposite directions due to bending of the beam, i.e. one is subjected to tensile stress and the other compressive stress; the two series connected elements behave like two series voltage sources. In the case of parallel connection, the electrical terminals are made through the top electrode and the bottom electrode. The two piezoelectric thin film elements connected in parallel behave like two current sources in parallel. In order to connect the two elements in parallel, the two elements need not to be separated physically by etching processing, but the top electrodes for each element need be separated during poling process so that opposite polarization can be produced for the two elements. After poling, the top electrodes can be connected by depositing a thin film conductive layer on the top of the two devices so that it serves as one electrical terminal. In this paper, for simplicity, we will focus on the first case with the coordinate system is shown in Fig. 2(a).

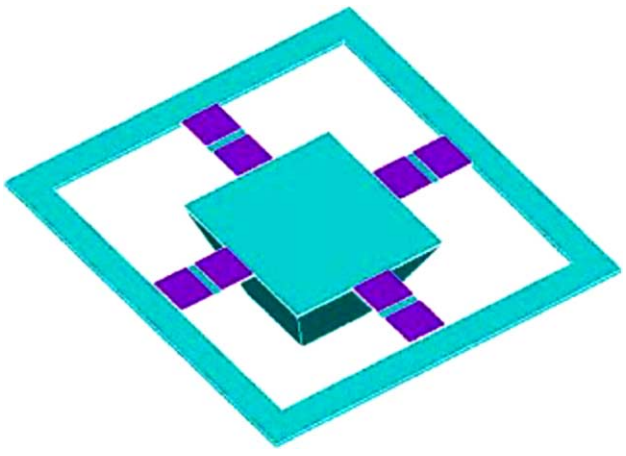

Fig. 1. A 3D view of the piezoelectric thin film microaccelerometer.

In practical fabrication of PZT thin film devices on silicon chip, sol–gel spin-on coating for PZT films is commonly used. A few micrometer up to 10 μm thick PZT films and their properties have been reported [15–18]. The piezoelectric PZT thin film devices are usually with the multilayer structure Pt/Ti/PZT/Pt/Ti/SiO_2/Si(1 0 0), in which Pt/Ti electrodes are very thin, typically from 100 to 150 nm. It is well known that the use of Ti thin film (∼10–40 nm) adhesion layer greatly promotes the bonding strength between the platinum layers with SiO_2 and PZT [19]. For simplicity, we ignore the effect of electrode layers in our analysis in this paper, with only PZT/Si two-layer structure for the suspended beams being considered for the thin film microaccelerometer modeling. The geometry of the accelerometer structure used for our modeling is given in Table 1.

Table 1
Component dimensions in a piezoelectric accelerometer

Length of suspension beam, l (μm)	400
Width of suspension beam, b (μm)	200
Thickness of suspension beam, h (μm)	5
Length of seismic mass, l_m (μm)	800
Thickness of seismic mass, h_m (μm)	300
Thickness of PZT film, h_{PZT} (μm)	0.5–5
Seismic mass, m (mg)	0.26

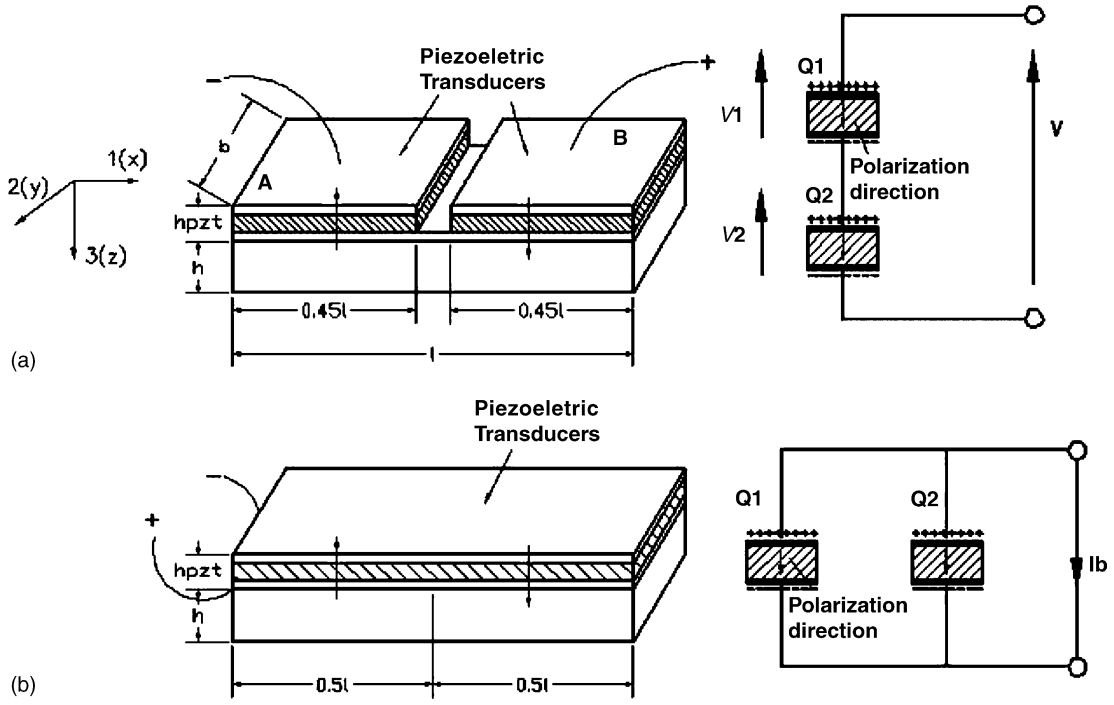

Fig. 2. Piezoelectric thin film elements are connected in (a) series or (b) in parallel.

The following assumptions are made in establishing the mechanical model of the PZT thin film microaccelerometer:

1. compared with the central seismic mass, the effective mass of the supporting beams is very small and can be ignored;
2. the seismic mass and rim of the structure are rigid;
3. both PZT and Si layers are elastic and obey Hooke's law;
4. the material of the piezoelectric transducer is orthotropic;
5. with the central mass only subjected to vertical acceleration and pure bending deformation generated in the suspended beams, the stresses in the 3-direction and strains in the 2-direction are negligible compared with the other strains and stresses. Therefore:

$$\sigma_3 = \sigma_5 = \sigma_6 = 0 \tag{1}$$

$$\varepsilon_2 = \varepsilon_4 = \varepsilon_6 = 0 \tag{2}$$

where the directions shown in Fig. 1, Voigt notation is used for the stresses as

$$\begin{pmatrix} \sigma_1 \\ \sigma_2 \\ \sigma_3 \\ \sigma_4 \\ \sigma_5 \\ \sigma_6 \end{pmatrix} = \begin{pmatrix} \sigma_{xx} \\ \sigma_{yy} \\ \sigma_{zz} \\ \sigma_{yz} \\ \sigma_{xz} \\ \sigma_{xy} \end{pmatrix} \tag{3}$$

and strains are ordered to be work conjugate.

When the sensor is subject to a normal acceleration $\ddot{z}$, the inertial force of the seismic mass induces a deflection of the beam suspension. Fig. 3 shows the schematic free-body diagram of one of the supporting beams. Because of the symmetry of the device structure, from the force equilibrium along the three-direction, we have the reaction force at O:

$$R_O = \tfrac{1}{4} m\ddot{z} \tag{4}$$

where m is the central mass. From the boundary condition and the symmetry of the structure, we get the bending moment $M(x)$ as

$$M(x) = \frac{1}{4} m\ddot{z}\left(\frac{l}{2} - x\right) \tag{5}$$

where l is the length of the beam.

Fig. 4 schematically shows cross-sectional area of the suspended PZT film/silicon beam, Y is the neutral axis of this section. Assuming that good bonding strength between PZT

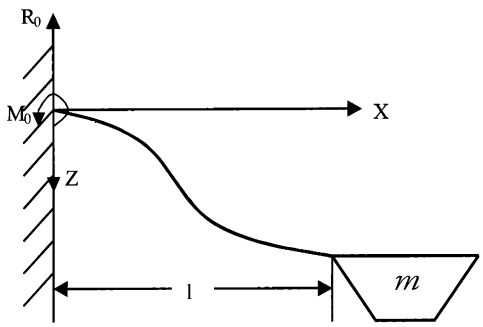

Fig. 3. Free-body diagram of the suspension beam.

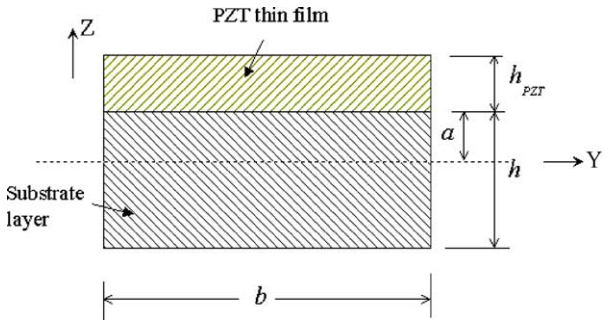

Fig. 4. Cross-sectional area of the suspended PZT/Si beam in the device.

thin film and the substrate beam, i.e. no strain discontinuity at the interface, the strain ε_1 can therefore be given by

$$\varepsilon_1 = \frac{z}{\rho} \tag{6}$$

where ρ is the radius of the curved surface. From the constitutive equation, we have

$$\sigma_i = C_{ij}\varepsilon_j, \quad i, j = 1, \ldots, 6 \tag{7}$$

where C_{ij} are the components of the fourth-order stiffness tensor. Based on the assumption 4, the stress σ_3 of the PZT film is given by

$$\sigma_3 = C_{31}\varepsilon_1 + C_{32}\varepsilon_2 + C_{33}\varepsilon_3 \tag{8}$$

Substituting Eqs. (1) and (2) into Eq. (8), we have

$$\varepsilon_3 = -\frac{C_{31}}{C_{33}}\varepsilon_1 \tag{9}$$

Therefore, the stress σ_1 of the PZT film can be written as

$$\sigma_1 = \left(C_{11} - \frac{C_{31}C_{13}}{C_{33}}\right)\varepsilon_1 \tag{10}$$

or

$$\sigma_1 = E_{\mathrm{P}}\varepsilon_1 \tag{11}$$

where

$$E_{\mathrm{P}} = C_{11} - \frac{C_{31}C_{13}}{C_{33}} \tag{12}$$

For simplicity, we assume that the silicon beam is isotropic, thus, the stress $\bar{\sigma}_1$ of the silicon beam is

$$\bar{\sigma}_1 = \frac{E_2}{1-\upsilon^2}\bar{\varepsilon}_1 \tag{13}$$

where $\bar{\varepsilon}_1$ is the strain of the silicon beam, E_2 and υ are the Young's modulus and Poisson's ratio of the beam respectively; or

$$\bar{\sigma}_1 = E_{\mathrm{B}}\bar{\varepsilon}_1 \tag{14}$$

where

$$E_{\mathrm{B}} = \frac{E_2}{1-\upsilon^2}$$

Now, we consider the cross-sectional area shown in Fig. 4. From the force equilibrium in one-direction, we have

$$\int_{-(h-a)}^{a} bE_{\mathrm{B}}\frac{z}{\rho}\,\mathrm{d}z + \int_{a}^{h_{\mathrm{PZT}}+a} bE_{\mathrm{P}}\frac{z}{\rho}\,\mathrm{d}z = 0 \tag{15}$$

$$\int_{-(h-a)}^{a} bE_{\mathrm{B}}\frac{z}{\rho}z\,\mathrm{d}z + \int_{a}^{h_{\mathrm{PZT}}+a} bE_{\mathrm{P}}\frac{z}{\rho}z\,\mathrm{d}z = M(x) \tag{16}$$

where a is the distance to the neutral axis in the substrate layer measured from the interface, b the width of the beam, h the thickness of the substrate layer, h_{PZT} the thickness of the PZT film, and $M(x)$ is the moment on the cross-sectional area. Therefore, from Eq. (15), we have

$$a = \frac{1}{2}\frac{E_{\mathrm{B}}h^2 - E_{\mathrm{P}}h_{\mathrm{PZT}}^2}{E_{\mathrm{B}}h + E_{\mathrm{P}}h_{\mathrm{PZT}}} \tag{17}$$

and from Eq. (16) the moment–curvature relationship is

$$\frac{1}{\rho} = \frac{M(x)}{(bE_{\mathrm{B}}/3)(h^3 - 3ah^2 + 3a^2h) + (bE_{\mathrm{P}}/3)(h_{\mathrm{PZT}}^3 + 3a^2h_{\mathrm{PZT}} + 3ah_{\mathrm{PZT}}^2)} \tag{18}$$

or

$$\frac{1}{\rho} = \frac{M(x)}{EI_{\mathrm{eq}}} \tag{19}$$

where

$$EI_{\mathrm{eq}} = \tfrac{1}{3}bE_{\mathrm{B}}(h^3 - 3ah^2 + 3a^2h) + \tfrac{1}{3}bE_{\mathrm{P}}(h_{\mathrm{PZT}}^3 + 3a^2h_{\mathrm{PZT}} + 3ah_{\mathrm{PZT}}^2) \tag{20}$$

Substituting Eqs. (6), (17) and (19) into Eq. (11), the average stresses in the PZT film σ_1 can be obtained as follows:

$$\sigma_1 = \frac{E_{\mathrm{P}}}{\rho}\left(\frac{h_{\mathrm{PZT}}}{2} + a\right) = \frac{E_{\mathrm{P}}M(x)}{EI_{\mathrm{eq}}}\left(\frac{h_{\mathrm{PZT}}}{2} + a\right) \tag{21}$$

If all the stresses other than that caused by bending in the piezoelectric films are negligible, the contribution from an infinitesimal portion of the piezoelectric material to the total charge for no external electrical field, D_3, is as follows:

$$D_3 = d_{31}\,\sigma_1 \tag{22}$$

where d_{31} is the piezoelectric coefficient. Substituting Eq. (21) into the integration of Eq. (22) over one suspension beam yields the charge output of piezoelectric films:

$$Q = \int_0^{0.45l} D_3 b\,\mathrm{d}x - \int_{0.55l}^{l} D_3 b\,\mathrm{d}x = 0.0619 d_{31} b\frac{E_{\mathrm{P}}}{EI_{\mathrm{eq}}}\left(\frac{h_{\mathrm{PZT}}}{2} + a\right) l^2 m\ddot{z} \tag{23}$$

So, the sensor's open-circuit voltage sensitivity S_V, defined as the ratio of the open-circuit voltage and acceleration:

$$S_V = \frac{V}{\ddot{z}} = \frac{Q}{\ddot{z}C}$$

can be obtained as

$$S_V = 0.0619 d_{31} b \frac{E_P}{EI_{eq}} \left(\frac{h_{PZT}}{2} + a \right) l^2 m / C \tag{24}$$

where C is the capacitance of two PZT thin film elements on one of the four suspended beams. Since the two PZT elements are connected in series, the capacitance is given by

$$C = \frac{0.45 \varepsilon_{33} lb}{2h_{PZT}} \tag{25}$$

where ε_{33} is the dielectric permittivity of PZT film.

Eq. (5) shows that maximum of $M(x)$ is at $x = 0$. It is assumed that with only vertical acceleration applied to the central seismic mass, causing pure bending deformation in the transducer beams, the piezoelectric film and silicon layer are then primarily subjected to stresses in the one-direction, and the other stresses are small and can be ignored, therefore, the maximum stress σ_{max} can be obtained either at the upper surface or at the lower surface. At the upper surface:

$$\sigma_{max1} = \frac{1}{8} \frac{E_P m \ddot{z} l}{EI_{eq}} (h_{PZT} + a) \tag{26a}$$

and at the lower surface:

$$\sigma_{max2} = \frac{1}{8} \frac{E_B m \ddot{z} l}{EI_{eq}} (h - a) \tag{26b}$$

Therefore, σ_{max} can be obtained by selecting the larger one of σ_{max1} and σ_{max2}.

2.2. Dynamic analysis

The dynamic model can be simplified as a beam with a large mass (half of the seismic mass m) in the center, and subjected to a periodic force $f(t)$, as shown schematically by Fig. 5. The sinusoidal force can be written as

$$f(t) = \tfrac{1}{2} mg \sin 2\pi f t \tag{27}$$

where $g = 9.8$ m/s and f is the driving frequency.

Assuming that the accelerometer is at rest initially, if only the first vibration mode is considered here, the general solution of the beam is given by [20]

$$z(x) = a_1 \cos(\beta x) + a_2 \sin(\beta x) + a_3 \cosh(\beta x) + a_4 \sinh(\beta x) \tag{28}$$

where a_1, a_2, a_3, a_4 and β are the constants. From the boundary conditions, the first normal mode of the accelerometer can be obtained as

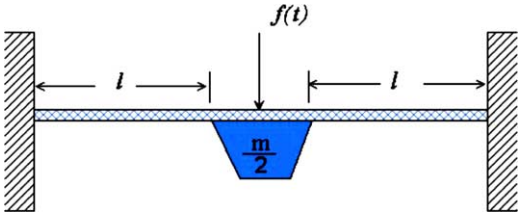

Fig. 5. Dynamic model of the accelerometer.

$$z_1(x) = V_a [\sin kx - \sinh(kx) + S(\cos kx - \cosh(kx))] = V_a g(x) \tag{29}$$

where $k = 4.73/2l$,

$$S = \frac{\sinh(kl) - \sin kl}{\cos kl - \cosh(kl)}$$

and V_a is the constant. Since the first normal is orthogonal, V_a can be obtained by

$$\int_0^{2l} \gamma(x) A(x) z_1^2(x)\, dx = 1 \tag{30}$$

where $\gamma(x)$ is the density and A is the cross-sectional area. Considering that the seismic mass m is much larger than the mass of the beams, the above equation can then be simplified to give

$$V_a = \sqrt{\frac{1}{m/2g^2(l)}} \tag{31}$$

From Rayleigh method, the fundamental natural frequency f_n is given by

$$f_n^2 = \frac{2}{4} \int_0^l \frac{dU_{max}}{\pi^2 K_{e\,max}} \tag{32}$$

where

$$K_{e\,max} = \tfrac{1}{2} m {z_1}^2(l)$$

For beam with single elastic layer, we have

$$dU_{max} = \frac{1}{2} \left(\frac{d^2 z_1}{dx^2} \right)^2 E_2 I_2 \tag{33a}$$

where

$$I_2 = \tfrac{1}{12} bh^3$$

and for the beam with both piezoelectric film and elastic layer:

$$dU_{max} = \frac{1}{2} \left(\frac{d^2 z_1}{dx^2} \right)^2 EI_{eq} \tag{33b}$$

Using the expansion theorem, the displacement of the accelerometer is

$$z(x, t) = z_1(x) \eta(t) \tag{34}$$

where $\eta(t)$ is the modal coordinate given by

$$\eta(t) = \frac{1}{2\pi f_n} \int_0^t N(\tau) \sin(2\pi f_n)(t - \tau)\, d\tau \tag{35}$$

where N is the modal force given by

$$N(t) = \int_0^{2l} z_1(x) f(x, t)\, dx \tag{36}$$

Substituting Eqs. (28), (35) and (36) into Eq. (34), we have

$$z(x, t) = \frac{V_a^2}{2} mgz(l) \frac{\sin 2\pi f t - (f/f_n) \sin 2\pi f_n t}{(2\pi f_n)^2 - (2\pi f)^2} \times [\sin kx - \sinh(kx) + S(\cos kx - \cosh(kx))] \tag{37}$$

Table 2
Mechanical properties of the piezoelectric accelerometer materials

	Silicon	PZT
Young's modulus (N/m^2)	1.9×10^{11}	C-matrix
Poisson's ratio	0.18	
Density (kg/m^3)	2330	7550
Dielectric constant ($K_3 = \varepsilon_{33}/\varepsilon_0$) ($\varepsilon_0 = 8.85 \times 10^{-12}$)	730	
Piezoelectric coefficient, d_{31} ($\times 10^{-12}$ C/N)		−93.5

So

$$\frac{1}{\rho} = \frac{\mathrm{d}^2 z}{\mathrm{d}x^2} \tag{38}$$

Therefore, the average stresses at the cross-sectional area of PZT film σ_1 can be obtained by Eq. (21). The charge output of piezoelectric films can then be calculated by Eq. (22),

$$Q = d_{31} b E_{\mathrm{P}} \left(\frac{h_{\mathrm{PZT}}}{2} + a \right) \frac{V_{\mathrm{a}}^2}{2} mg\ddot{z}(l) \times \frac{\sin 2\pi f t - (f/f_{\mathrm{n}}) \sin 2\pi f_{\mathrm{n}} t}{(2\pi f_{\mathrm{n}})^2 - (2\pi f)^2} \times [T(0.45l) - T(0) - T(l) + T(0.55l)] \tag{39}$$

where

$$T(x) = k\,[-S \sinh(kx) - S \sin kx + \cos kx - \cosh(kx)] \tag{40}$$

Using Eq. (39), the charge output, $Q/\ddot{z}$, of the device under dynamic excitation can be predicted.

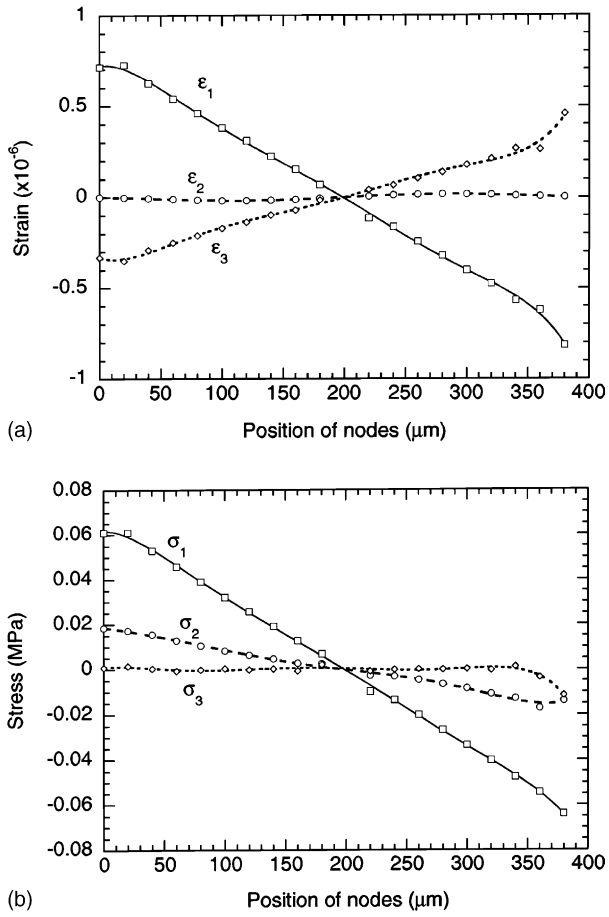

Fig. 6. Stress and strain distribution of PZT film along path A–B: (a) the strain distribution; (b) the stress distribution.

$$[C^{\mathrm{E}}] = \begin{bmatrix} 11.425 & 5.8294 & 5.8525 & 0 & 0 & 0 \\ 5.8294 & 11.425 & 5.8525 & 0 & 0 & 0 \\ 5.8525 & 5.8525 & 9.8181 & 0 & 0 & 0 \\ 0 & 0 & 0 & 2.0747 & 0 & 0 \\ 0 & 0 & 0 & 0 & 2.0747 & 0 \\ 0 & 0 & 0 & 0 & 0 & 2.6042 \end{bmatrix} \times 10^{10}\ (\mathrm{N/m^2}) \tag{41}$$

3. Finite element analysis

3.1. Static behavior of the microaccelerometer

A finite element solution (ANSYS 5.7) is used for comparison to the analytical result. Table 1 shows typical dimensions of the beams of a piezoelectric accelerometer. Table 2 lists the materials properties used in calculation. The piezoelectric, dielectric and elastic properties of PZT thin films reported in the literature have a strong dependence on the processing methods used to fabricate the films. Not all the necessary properties are available. Therefore, properties of bulk PZT ceramics are used in our calculation. The stiffness coefficient matrix of PZT is shown in Eq. (41), which is cited from [13]:

When an acceleration $\ddot{z} = 1\,g$ is applied on the accelerometer, the stress and strain of PZT film in the x-, y-, z-directions along path A–B (Fig. 2(a)) obtained by finite element analysis are shown in Fig. 6(a) and (b). It is clear that that the stress in the z-direction and the strain in the y-direction are negligible compared with the other strains and stresses, which agrees with assumption (5) in Section 2.

The dependence of the open-circuit voltage sensitivity of the microaccelerometer on the device geometry is calculated by both the analytical equation and by finite element modeling. The results are plotted in Figs. 7–10, and show that finite element results are in good agreement with the analytical results. Since the sensitivity is proportional to the effective mass, as indicated by Eq. (24), the ignorance of the effective mass of the four transducer beam lead to the slightly smaller analytical sensitivity values than the results by FEM. With the increase of thickness and width of the

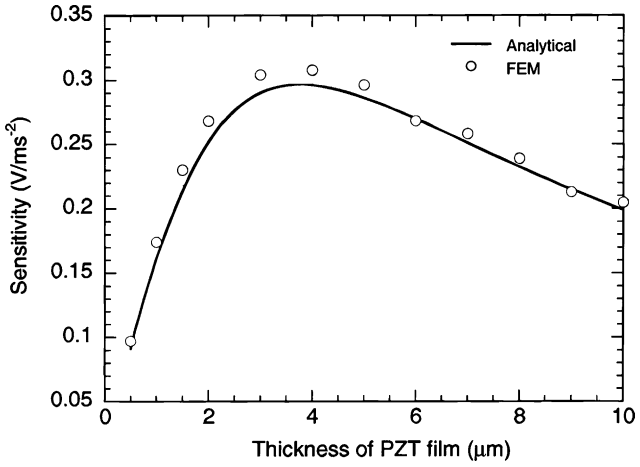

Fig. 7. The accelerometer sensitivity as a function of the thickness of the PZT film ($l = 400\,\mu m$, $b = 200\,\mu m$, $h = 5\,\mu m$, $E_2 = 190\,GPa$).

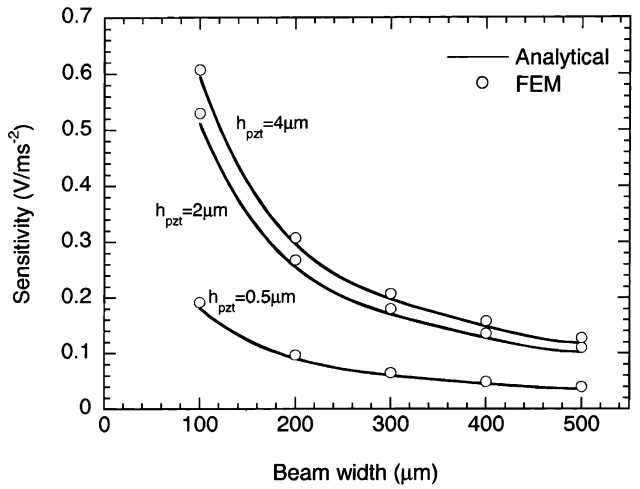

Fig. 8. The accelerometer sensitivity in terms of the beam width ($l = 400\,\mu m$, $h = 5\,\mu m$, $E_2 = 190\,GPa$).

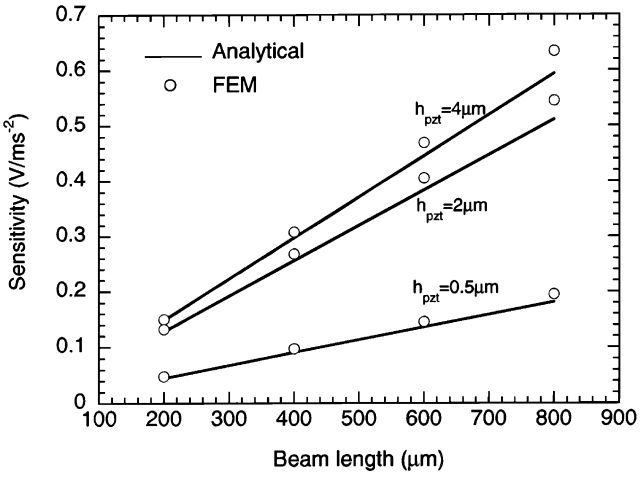

Fig. 9. The accelerometer sensitivity as a function of the beam length ($b = 200\,\mu m$, $h = 5\,\mu m$, $E_2 = 190\,GPa$).

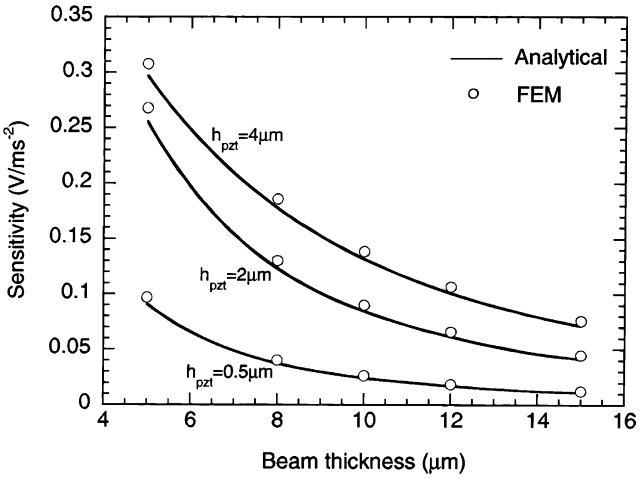

Fig. 10. The accelerometer sensitivity as a function of the beam thickness ($l = 400\,\mu m$, $b = 200\,\mu m$, $E_2 = 190\,GPa$).

suspended beam structure, the accelerometer sensitivity decreases; while with the increases of the beam length, sensitivity increases. It should be pointed out that the open-circuit voltage sensitivity defined by Eq. (24) is the ratio of the generated change and the sensor capacitance under applied 1 g acceleration. In practical measurement, the generated charge would be collected on the finite loading capacitance in parallel to the sensor. Since the generated charge is proportional to the beam width b, with increasingly small values of beam width b, the generated charge tends to zero, thus the actually sensitivity will approach to zero. In this case, it will be better to use charge sensitivity, $S_Q = Q/\ddot{z}$, rather than open-circuit voltage sensitivity.

If all the parameters are kept fixed except the PZT film thickness, it is found that an increase of the thickness of PZT layer caused a sensitivity increase, reaches a maximum value at an appropriate thickness, and then decreases with further increases of PZT thickness (Fig. 7). The reason for this behavior is that, Eqs. (20) and (21) show that with the increase of the thickness of PZT layer, EI_{eq} and $(h_{PZT}/2 + a)$ both increase, but the increase of EI_{eq} is less than that of $(h_{PZT}/2 + a)$ initially, so sensitivity increases. However, the power of the PZT film thickness in EI_{eq} and $(h_{PZT}/2+a)$ is 3 and 1, respectively, so with further increase of PZT thickness h_{PZT}, the value of EI_{eq} gradually matches and then exceeds that of $(h_{PZT}/2 + a)$, which makes sensitivity reach a maximum value, then drop. From Eq. (16), the distance between the neutral axis and the interface of the beam and PZT can be found to be approximately 1.3 μm, which means the neutral axis in the beam is close to the interface of the beam and PZT. This is an important result, which can be used as a guideline to choose the appropriate PZT layer thickness to achieve high sensitivity of the accelerometer.

It should be pointed out that besides silicon, other elastic materials could also be used for the beam to design and fabricate the microaccelerometer. Fig. 11 shows the depen-

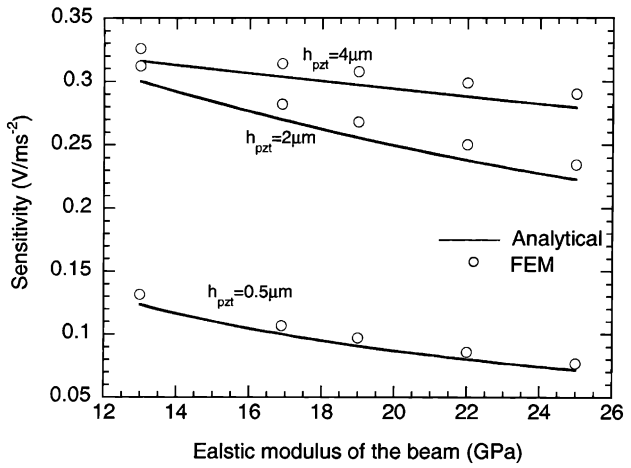

Fig. 11. The change in accelerometer sensitivity with changing elastic modulus of the beam ($l = 400\,\mu m$, $b = 200\,\mu m$, $h = 5\,\mu m$).

dence of the devices' sensitivities with respect to the elastic modulus of the beam for microaccelerometers with various PZT layer thickness. Again, the finite element results are in good agreement with the analytical results.

From Eq. (26), it can be seen that the maximum stress of the accelerometer is proportional to the magnitude of the input acceleration. Therefore, in the design of the accelerometer, the increase of sensitivity is limited by the maximum allowable stress of the beam structure. If we assume the central mass is subjected to a sinusoidal vibration with vertical displacement $z = z_0 \sin(\omega t + \phi_0)$, the acceleration will be:

$$\ddot{z} = \frac{d^2 z}{dt^2} = -z_0 \omega^2 \sin(\omega t + \phi_0)$$

i.e. the amplitude of the acceleration is a quadratic function of oscillation frequency. Depending on the vibration frequency and displacement of the central mass of the accelerometer, the amplitude of acceleration could be very high. For example, for a piezoelectric thin film accelerometer with 5 μm Si substrate layer, 4 μm PZT film, and other dimensions given in Table 1, the fundamental resonant frequency has been obtained to be approximately 10.5 kHz by FEM. Using the yield stress of 75 MPa for bulk ceramic PZT for estimation, the maximum acceleration that can be measured by the microaccelerometer is about 1220 g, which is very large acceleration. If the amplitude of the vibration displacement (z_0) is 25 μm, the upper frequency for the accelerometer is about 3450 Hz, which is about one-third of the natural frequency of the accelerometer.

If the device is subjected to mechanical excitation with large vibration amplitude, the upper operating frequency should be reduced to maintain good reliability of the devices. Therefore, depending on the application conditions, compromises between device's sensitivity, operating frequency range and reliability need to be balanced. Increasing both beam and PZT film thickness can enhance the device reliability, and enable the device being used for large acceleration measurement.

Table 3
The resonant frequencies of the accelerometer (FEM) ($l = 400\,\mu m$, $b = 200\,\mu m$, $h = 5\,\mu m$, $h_{PZT} = 0.5\,\mu m$, $E_2 = 190\,GPa$)

Mode	Natural frequencies, f_n (kHz)
1	5.783
2	10.934
3	10.972
4	278.27
5	278.78

3.2. FEM analysis of dynamic behavior of the microaccelerometer

The ANSYS 5.7 Block-Lanczos solver is used for the modal analysis. The frequencies from the first to fifth mode obtained by FEM are listed in Table 3 and the corresponding modes are shown in Fig. 12 . From Eq. (32), the analytical result of the fundamental resonant frequency can be calculated as 5.858 kHz, which agrees fairly well with the result by FEM simulation, 5.783 kHz. The slightly larger value of fundamental resonance frequency by analytical method

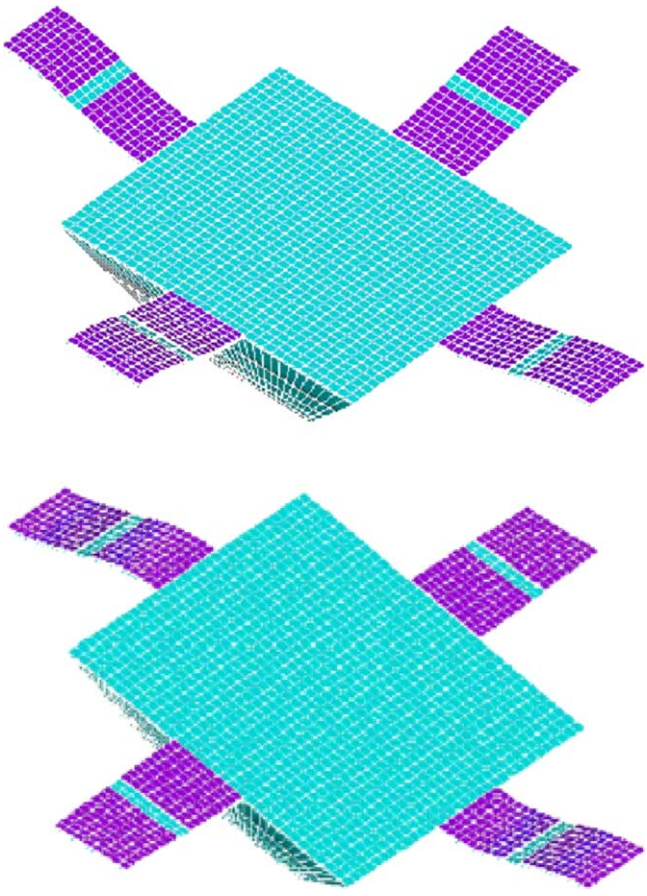

Fig. 12. The first five modes of the accelerometer.

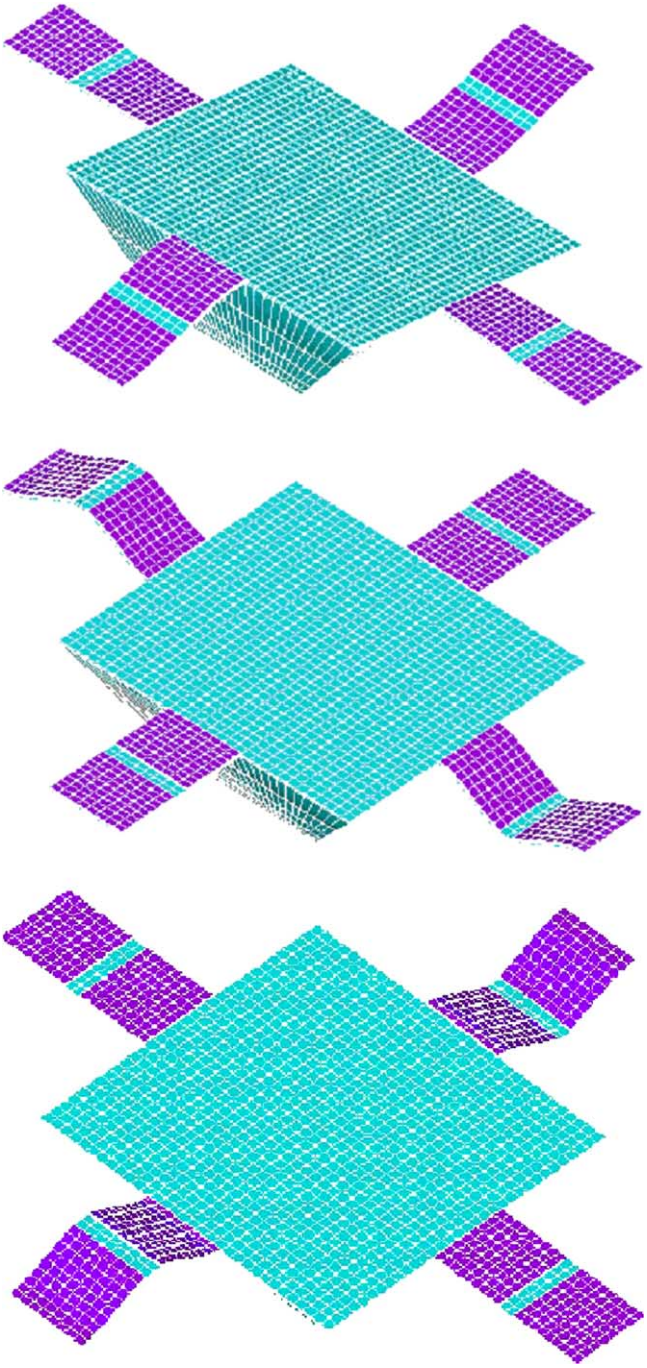

Fig. 12. (*Continued*)

is due to ignorance of the effective mass of the transducer beams (assumption (1) in Section 2.1). Fig. 12(a) shows that the first mode is a bending mode, in which four beams have the same deformation, so they have the same output charge. The second and third modes are that the accelerometer is subjected to the torsion, which have no output charge because of the skew-symmetrical deformation. The fourth mode and fifth mode, which have frequencies over 200 kHz, have little effect under a relatively low driving frequency, so the first mode plays the major role on the output charge,

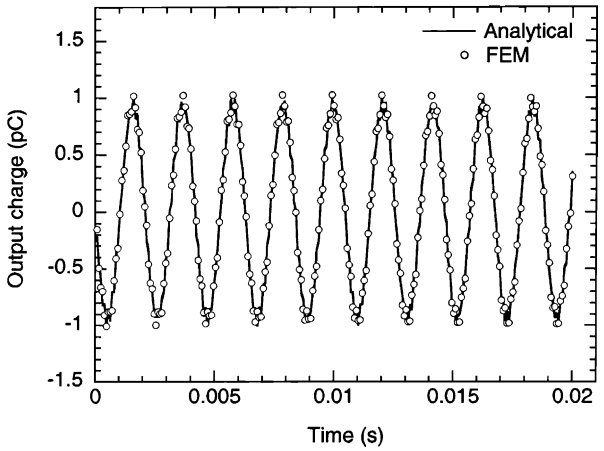

Fig. 13. Accelerometer output charge as a function of time at excitation frequency $f = 478$ Hz.

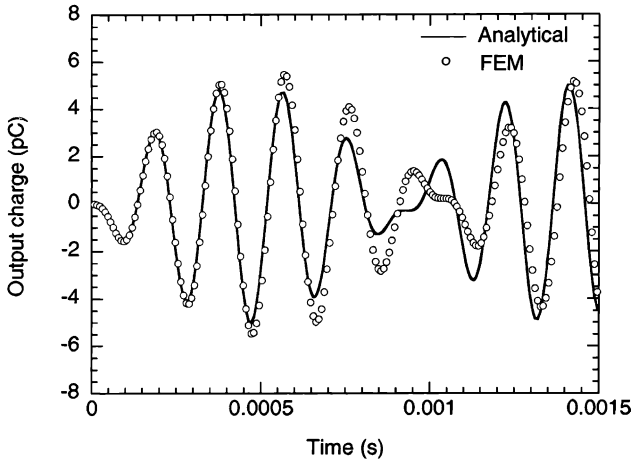

Fig. 14. Accelerometer output charge as a function of time at excitation frequency $f = 4778$ Hz.

which supports the assumption that the first mode vibration is only considered.

Figs. 13–15 show that the response of the accelerometer is periodic when it is subject to a periodic force. Again the FEM results agree well with the analytical results. Tables 4 and 5 show that with the increase of the driving frequency, there is little change of the output charge, but when the driving frequency is close to the fundamental resonant frequency, the output charge and the corresponding maximum

Table 4
Variation of the maximum output charge with different driving frequencies

Driving frequencies (Hz)	Output maximum charge (pC)	
	FEM	Analytical
4.78	0.939	0.935
47.78	0.943	0.935
477.8	1.02	1.00
4778	5.52	5.02
47777	0.125	0.123

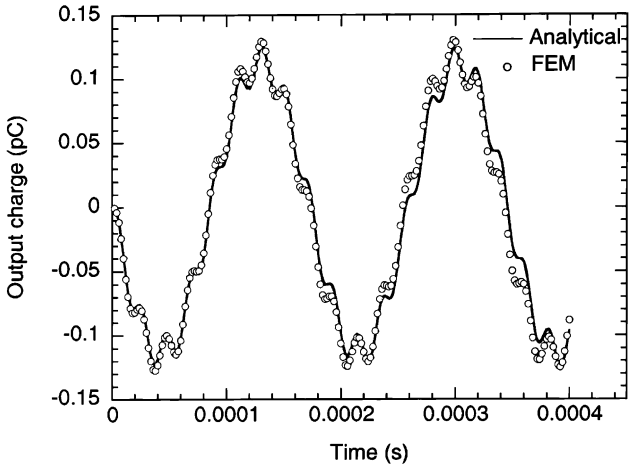

Fig. 15. Accelerometer output charge as a function of time at excitation frequency $f = 4777$ Hz.

Table 5
Variation of the maximum stress with different driving frequencies

Driving frequencies (Hz)	Maximum stress (MPa)	
	FEM	Analytical
4.78	0.125	0.144
47.78	0.126	0.144
477.8	0.137	0.151
4777.7	0.734	0.774
47777	0.0168	0.0201

stress become much larger, after this stage, the output charge drops to a very small value, therefore, it is reasonable that the typical range of the accelerometer frequency is chosen lower than $f_n/5$ or $f_n/3$ [5]. However, in case that a large charge output is required, the accelerometer frequency can be selected around f_n, but in the meantime, the safety of the structure should be considered.

From Eq. (32), the relation between the fundamental resonant frequency and the thickness of the PZT film can be obtained as shown in Fig. 16, which states that with the increase of PZT film thickness, the fundamental resonant frequency also increases. Figs. 16 and 7 provide the base for selecting a suitable thickness of the PZT films while an accelerometer is designed.

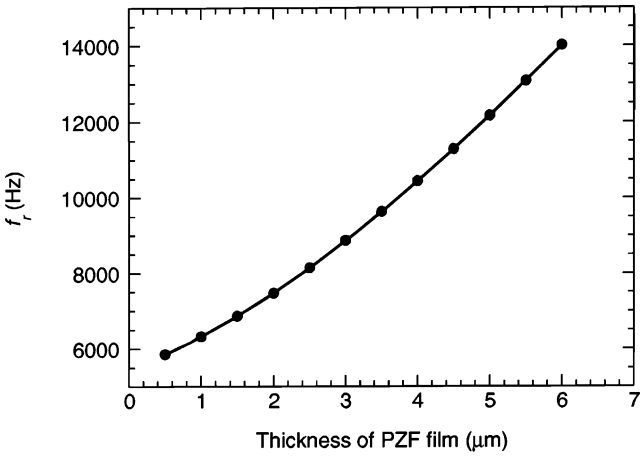

Fig. 16. The fundamental resonant frequency as a function of the thickness of PZT thin films ($l = 400\,\mu$m, $b = 200\,\mu$m, $h = 5\,\mu$m, $E_2 = 190$ GPa).

4. Conclusion

In this paper, an analytical method and the FEM have been applied to study the static and dynamic behavior of a piezoelectric microaccelerometer. The analytical results on the devices' sensitivity and resonant frequencies are in good agreement with the results simulated by FEM. This suggests that analytical results can be a fairly reliable guide to the design and calculation of the accelerometer structure. The static study found that increasing the beam width, thickness, or the Young's modulus, decreases the accelerometer sensitivity (S_V). Increasing the length of the beam increases S_V. For a fixed substrate layer thickness, increasing of the thickness of the PZT film can increase S_V up to a point and further increases reduce the sensitivity. Therefore, an optimal thickness ratio for PZT thin film and substrate layer should be considered in the device fabrication for high sensitivity. The estimation of the stress distribution also provides a guideline in device design for device reliability. For the accelerometer structure, the dynamic analysis found that when the driving frequency is close to the fundamental resonant frequency, the output charge and the corresponding maximum stress become much larger; otherwise the output charge is relatively small. Therefore, it is reasonable that the typical range of the accelerometer frequency is chosen below one-third or one-fifth of the natural frequency. This study can be readily applied for design and fabrication of the on-chip piezoelectric microaccelerometer to achieve high sensitivity and broad operating frequency range.

Acknowledgements

The authors would like to acknowledge the financial support from the University of Pittsburgh Small Grant Funding.

References

[1] G. Gautschi, Piezoelectric Sensorics: Force, Strain, Pressure, Acceleration and Acoustic Emission Sensors, Materials and Amplifiers, Springer, Berlin, 2002.
[2] K. Uchino, Piezoelectric Actuators and Ultrasonic Motors, Kluwer, Boston, 1996.
[3] G.A. Macdonald, A review of low cost accelerometers for vehicle dynamics, Sens. Actuators A 21–23 (1990) 303–307.
[4] K. Kunz, P. Enoksson, G. Stemme, Highly sensitive triaxial silicon accelerometer with integrated PZT thin film detectors, Sens. Actuators A 92 (2001) 156–160.
[5] S.P. Beeby, N.J. Grabham, N.M. White, Microprocessor implemented self-validation of thick-film PZT/silicon accelerometer, Sens. Actuators A 92 (2001) 168–174.

[6] V.K. Varadan, V.V. Varadan, H. Subramanian, Fabrication, Sens. Actuators A 90 (2001) 7–19.
[7] D. Crescini, D. Marioli, E. Sardini, A. Taroni, Large bandwidth and thermal compensated piezoelectric thick-film acceleration transducer, Sens. Actuators A 87 (2001) 131–138.
[8] Y. Nemirovsky, A. Nemirovsky, P. Muralt, N. Setter, Design of a novel thin-film piezoelectric accelerometer, Sens. Actuators A 56 (1996) 239–249.
[9] H.G. Yu, L. Zou, K. Deng, R. Wolf, S. Tadigadapa, S. Trolier-McKinstry, Lead zirconate titanate MEMS accelerometer using interdigitated electrodes, Sens. Actuators A 107 (2003) 26–35.
[10] A. Spineanu, P. Bénabès, R. Kielbasa, A digital piezoelectric accelerometer with sigma–delta servo technique, Sens. Actuators A 60 (1997) 127–133.
[11] D. Eicher, M. Giousouf, W. von Munch, Measurement on micromachined silicon accelerometers with piezoelectric sensor action, Sens. Actuators A 75 (1999) 247–252.
[12] L. Ries, W. Smith, Finite element analysis of a deformable array transducer, IEEE Trans. Ultrason. Ferroelectr. Freq. Contr. 46 (1999) 1352–1363.
[13] J. Yu, C. Lan, System modeling of microaccelerometer using piezoelectric thin films, Sens. Actuators A 88 (2001) 178–186.
[14] V. Ferrari, D. Marioli, A. Taroni, Theory, modeling and characterization of PZT-on-alumina resonant piezo-layers as acoustic-wave mass sensors, Sens. Actuators A 92 (2001) 182–190.
[15] B. Xu, L.E. Cross, J.J. Bernstein, Ferroelectric and antiferroelectric films for microelectromechanical systems applications, Thin Solid Films 377/378 (2000) 712–718.
[16] H.D. Chen, K.R. Udayakumar, C.J. Gaskey, L.E. Cross, Fabrication and electrical properties of lead zirconate titanate thick films, J. Am. Ceram. Soc. 79 (1996) 2189.
[17] Y.L. Tu, S.J. Milne, Processing and characterization of PZT films up to 10 μm thick, J. Mater. Res. 11 (1996) 2556–2564.
[18] R. Kurchania, S.J. Milne, Characterisation of sol–gel PZT films in the thickness range 0.25–10 microns, J. Mater. Res. 14 (1999) 1852–1859.
[19] N. Ledermann, P. Muralt, J. Baborowski, S. Gentil, K. Mukati, M. Cantoni, A. Seifert, N. Setter, {1 0 0}-textured, piezoelectric $Pb(Zr_x, Ti_{1-x})O_3$ thin films for MEMS: integration, deposition and properties, Sens. Actuators A 105 (2003) 162–170.
[20] H. McCallion, Vibration of Linear Mechanical Systems, Longman Group, London, 1973, p. 103

Biographies

Qing-Ming Wang is an assistant professor in the Department of Mechanical Engineering, University of Pittsburgh, Pittsburgh, PA. He received the BS and MS degrees in materials science and engineering from Tsinghua University, Beijing, China, in 1987 and 1989, respectively; and the PhD degree in materials from the Pennsylvania State University, University Park, PA, in 1998. His primary research interests are in microelectromechanical systems (MEMS) and microfabrication; smart materials; and piezoelectric/electrostrictive ceramics, thin film and composites for electromechanical transducer and actuator and sensor applications. He is a member of IEEE, IEEE-UFFC, the Materials Research Society (MRS), the American Society of Mechanical Engineers, and the American Ceramic Society.

Zhaochun Yang received his BS and MS degrees in mechanical engineering from Beihang University, and University of Petroleum (Beijing) in 1991 and 1994, respectively. He is currently a PhD candidate in the Department of Mechanical Engineering, University of Pittsburgh. His research interests include finite element modeling of electromechanical structures and devices, and the development of new computational simulation methods and the application of computational methods to problems in biomechanics.

Fang Li received the BS and MS degrees from the Department of Precision Instruments and Mechanology, Tsinghua University, Beijing, China, in 1999 and 2002, respectively. She is currently a PhD candidate in the Department of Mechanical Engineering, University of Pittsburgh, Pittsburgh, PA. Her primary research interests include piezoelectric devices for sensor and actuator applications, and surface acoustic wave (SAW) and bulk acoustic wave (BAW) sensors for biological applications.

Patrick Smolinski is an associate professor in the Department of Mechanical Engineering, University of Pittsburgh, Pittsburgh, PA. He received PhD degree in theoretical and applied mechanics from Northwestern University in 1985. His research interests include the development of new computational simulation methods and the application of computational methods to problems in manufacturing and biomechanics. He currently involved with research projects in the extended finite method for modeling solidification processes, the finite element modeling of sheet metal forming, modeling the flow of granular material, stress analysis and design of ankle replacement components and the study of the wear of polyethylene joint components.